Macromolecules

Article

Cite This: Macromolecules 2018, 51, 468−479

Tuning the Properties and Self-Healing Behavior of Ionically Modified Poly(isobutylene-*co*-isoprene) Rubber

Marcus Suckow,[†] Anton Mordvinkin,[∥] Manta Roy,[‡] Nikhil K. Singha,[‡] Gert Heinrich,[†] Brigitte Voit,[†,§] Kay Saalwächter,*[,∥] and Frank Böhme*[,†]

[†]Leibniz-Institut für Polymerforschung Dresden e.V., Hohe Straße 6, Dresden, Germany

[‡]Rubber Technology Centre, Indian Institute of Technology, Kharagpur 721302, India

[§]Organische Chemie der Polymere, Technische Universität Dresden, D-01062 Dresden, Germany

[∥]Institut für Physik−NMR, Martin-Luther-Universität Halle-Wittenberg, Betty-Heimann-Str. 7, 06120 Halle (Saale), Germany

Supporting Information

ABSTRACT: The focus of this work is on the nature of self-healing of ionically modified rubbers obtained by reaction of brominated poly(isobutylene-*co*-isoprene) rubber (BIIR) with various alkylimidazoles such as 1-methylimidazole, 1-butylimidazole, 1-hexylimidazole, 1-nonylimidazole, and 1-(6-chlorohexyl)-1*H*-imidazole. Based on stress−strain and temperature dependent DMA measurements, a structural influence of the introduced ionic imidazolium moieties on the formation of ionic clusters and, as a consequence, on the mechanical strength and self-healing behavior of the samples could be evidenced. These results are fully supported by a molecular-level assessment of the network structure (cross-link and constraint density) and the dynamics of the ionic clusters using an advanced proton low-field NMR technique. The results show distinct correlations between the macroscopic behavior and molecular chain dynamics of the modified rubbers. In particular, it is shown that the optimization of material properties with regard to mechanical and self-healing behavior is limited by opposing tendencies. Samples with reduced chain dynamics exhibit superior mechanical behavior but lack on self-healing behavior. In spite of these limitations, the overall performance of some of our samples including self-healing behavior exceeds distinctly that of other self-healing rubbers described in the literature so far.

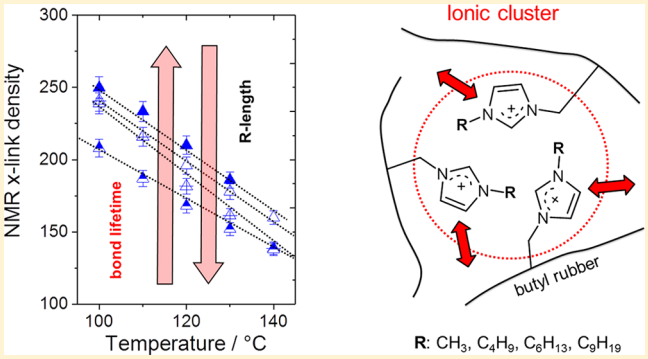

INTRODUCTION

Recently, the description of a self-healing rubber by Leibler et al.[1] initiated a new innovative trend in polymer research. Based on the author's idea to build up a rubber-like material by utilizing dynamic hydrogen bonds, a couple of new approaches have been described. Some approaches are based upon similar building blocks as in Leibler's original work,[2−4] while other approaches are based on principles known from supramolecular chemistry, such as homo- and heterocomplementary hydrogen bonding.[5,6] Recently, more and more efforts have been devoted to the implementation of self-healing properties on commercially available rubbers such as natural rubber,[7−9] polybutadiene,[10] acrylonitrile−butadiene rubber,[11] chloroprene rubber,[12] styrene−butadiene rubber, and polydimethylsiloxane.[2,13] In order to facilitate self-healing, both physical[10,11,13] and reversible covalent cross-linking[7−9,12] have been utilized in these rubber systems.

As impressive as the self-healing properties of the introduced rubber systems might be, their overall mechanical performance has to be taken into account with regard to potential applications. With tensile strength values smaller than 3 MPa, often even distinctly smaller than 1 MPa, their technical relevance has to be put into perspective. Pronounced self-healing properties were frequently demonstrated and discussed on the example of rubbers with low overall performances, suggesting that self-healing was the result of insufficient cross-linking causing long-time creep. In this regard, sometimes quite controversial opinions about the self-healing capability and mechanisms of certain rubber materials are discussed.[14,15] The development of a self-healing rubber with acceptable overall performances requires a deeper understanding of how the kind and quantity of reversible cross-links affect the mutual dependence of mechanical strength and self-healing behavior.

In our own research concerning self-healing rubbers, the focus has been on ionically modified brominated poly(isobutylene-*co*-isoprene) (BIIR), also known as bromobutyl rubber. BIIR is a well-established synthetic rubber which is obtained by bromination of butyl rubber (IIR). The higher

Received: October 28, 2017
Revised: December 14, 2017
Published: December 29, 2017

DOI: 10.1021/acs.macromol.7b02287
Macromolecules 2018, 51, 468−479

Scheme 1. Ionic Modification of Bromobutyl Rubber by Conversion with Alkylimidazoles

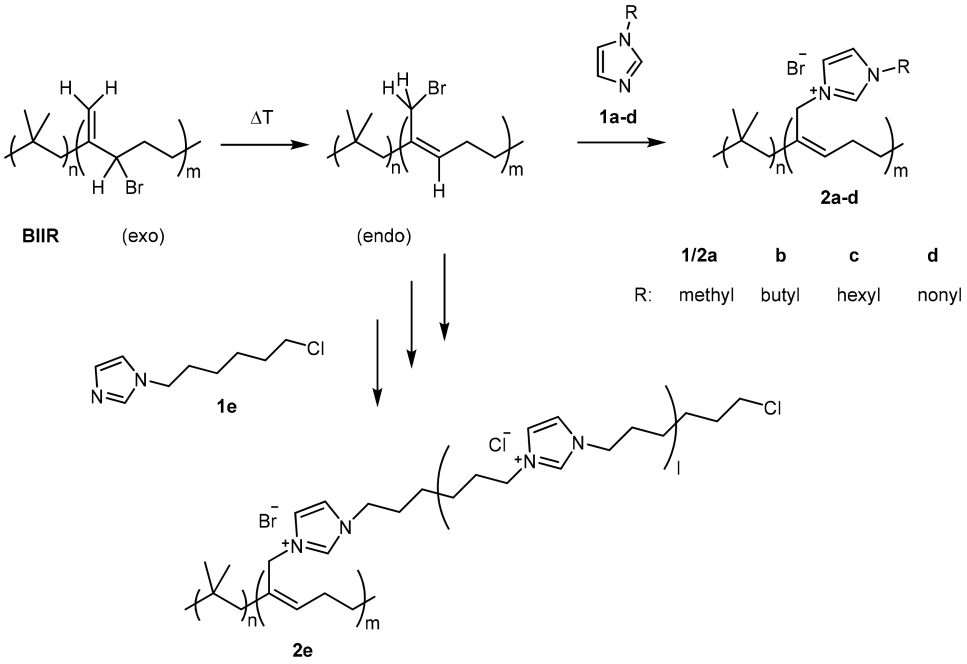

reactivity of the allylic bromide groups in BIIR facilitates sulfur curing. Furthermore, BIIR shows higher compatibility with unsaturated polymers and enhanced adhesion compared to IIR. At the same time, bromination provides improved air impermeability, which predestines BIIR as a potential material for tire inner liners. On the other hand, the reactive allylic bromide groups open up various opportunities for functionalization. Nucleophilic substitution reactions with amines,[16,17] carboxylate nucleophiles,[18,19] cyclic amidines,[17] and *N*-alkylbenzaldimines[20] are well described by Parent et al. An interesting approach comprises alkylation reactions with PPh_3, tertiary amines, and imidazoles which result in the formation of ionic groups.[21,22] Interactions of these groups may lead to physical cross-linking of the rubber. Owing to the reversibility of ionic interactions, ionically modified polymers and elastomers have gained increasing interest in developing self-healing materials.[10,23−27] The formation, rearrangements, and regeneration of ionic clusters may contribute to self-healing processes in the case of material damage.

Recently, we have reported about the self-healing behavior of ionically modified BIIR[28] and related blend composites.[29−31] For this, BIIR was reacted with 1-butylimidazole as described first by Parent et al.[21,22] The imidazolium ions originated by this reaction formed a noncovalent network with considerable mechanical strength. Because of the dynamic character of the ionic interactions, the material exhibited pronounced self-healing behavior.

It is reasonable to assume that the properties of ionically modified BIIR depend on the size and strength (compactness) of the ionic clusters formed as a result of the interactions of the ionic groups. Since ionic interactions are dynamic in nature, the cluster size is in principle variable. It can be affected by thermal history, processing, and deformation. Furthermore, it depends on the mobility and the number of the ionic groups and their interactions within the clusters. Since the concentration of bromide groups in BIIR is small (1−1.5 mol %), the number of ionic groups that can be produced by the conversion with alkylimidazoles is limited. As recently shown by us, one possibility to increase the number of ionic groups in BIIR was to blend it with a reactive poly(ionic liquid).[31] However, covalent cross-linking during mixing exerted a negative influence on the overall performance of the rubber.

In this article, we describe the ionic modification of BIIR by conversion of the bromide groups with various alkylimidazoles according to Scheme 1. While the reaction with the simple alkylimidazoles **1a−1d** leads to the formation of individual substituents, the reaction with the polymerizable 1-(6-chlorohexyl)-1*H*-imidazole[32] (**1e**) produces ionic grafts of variable length. This implies differences in mechanical and self-healing behavior of the modified samples. Based on mechanical tests, DMA, and dedicated solid-state NMR studies, the structural influence on the formation of ionic clusters and their influence on both network formation and self-healing behavior are discussed. The investigations are aimed at identifying correlations between macroscopic properties, molecular dynamics, and self-healing behavior, whereby particularly low-field multiple-quantum (MQ) NMR experiments contribute to a better understanding of molecular influences on the network formation and its dynamics.

EXPERIMENTAL SECTION

Materials. Imidazole (puriss p.a., ≥99.5%), 1-methylimidazole (99%), 1-butylimidazole (98%), 1-bromohexane (96%), 1-bromononane (98%), 1-bromo-6-chlorohexane (99%), and sodium amide (98%) from Sigma-Aldrich, methylene chloride (p.a.), toluene (p.a.), and THF (p.a.) from Acros Organics, and $CDCl_3$ (≥99.8%) from Euriso-top were used as received. BIIR with a bromine content of 1.13 wt % (0.139 mmol/g allylic bromide, ^{1}H NMR; see Supporting Information: S1) was a commercial product of Lanxess.

Synthesis of Alkylimidazoles (1c−1e). The alkylimidazoles were synthesized by conversion of imidazole with respective alkyl bromides in the presence of $NaNH_2$ and purified by column chromatography as recently published.[32] For **1e**, 1-bromo-6-chlorohexane was used.

1c/d. Yield: 86−95%. ^{1}H NMR ($CDCl_3$) δ_H ppm: 7.45 (1H, Im), 7.05 (1H, Im), 6.89 (1H, Im), 3.92 (2H, N−CH_2), 1.77 (2H, N−

DOI: 10.1021/acs.macromol.7b02287
Macromolecules 2018, 51, 468−479

CH_2-CH_2), 1.32−1.23 (2nH, $(CH_2)_n-CH_3$), 0.88 (3H, CH_3) (see Supporting Information: S2 and S3).

1e. Yield: 67%. ^{1}H NMR ($CDCl_3$) δ_H ppm: 7.44 (1H, Im), 7.04 (1H, Im), 6.89 (1H, Im), 3.93 (2H, N−CH_2), 3.51 (2H, CH_2−Cl), 1.82−1.72 (4H, N−CH_2−CH_2, CH_2−CH_2−Cl), 1.46 (2H, CH_2), *1.31 (2H, CH_2)* (see Supporting Information: S4).

Ionic Modification of BIIR by Conversion with Alkylimidazoles (2a−2e). The synthesis of ionically modified BIIR in the melt and in solution is demonstrated for **2b** and **2e$_s$** as examples. In order to achieve high conversion of bromide groups in the melt, a 1.5-fold excess of **1a−1d** was added to BIIR. For the conversion with the polymerizable **1e** the amount of modifier was varied as described in Table 1.

Table 1. Sample Overview

	polymer preparation		polymer composition			
sample	M[a]	[M]:[Br][b]	GD[c]	Br_I/Cl_I[d]	Br_t/Cl_t[e]	L[f]
2a	**1a**	1.5	>0.95			1
2b	**1b**	1.5	>0.95			1
2c	**1c**	1.5	>0.95			1
2d	**1d**	1.5	>0.95			1
2e$_s$[g]	**1e**	1.0	0.59	1.28	0.39	1.1
2e$_i$	**1e**	1.0	0.19	3.50	1.70	1.2
	after 2 months		0.19	3.01	1.56	1.5
2e$_{ii}$	**1e**	1.5	0.25	0.67	0.23	2.1
	after 2 months		0.30	0.48	0.12	2.2
2e$_{iii}$	**1e/1b**	1.5/1.0	0.45	0.41	0.12	1.9
	after 2 months		0.58	0.27	0.09	2.0

[a]Alkylimidazole used for modification. [b]Molar ratio of alkylimidazole in the reaction mixture related to the molar content of allylic bromide. [c]Grafting degree GD determined by ^{1}H NMR. [d]Ratio of Br and Cl substituted isoprene units determined by ^{1}H NMR. [e]Ratio of Br and Cl terminal groups determined by ^{1}H NMR. [f]Average grafting length determined by ^{1}H NMR. [g]Synthesized in $CHCl_3$, 3 days at RT, 3 days at 65 °C. All other samples were grafted in the melt.

*In the Melt (**2b**).* An amount of 50 g of BIIR (6.94 mmol of allylic bromide) and 1.5 mL of **1b** (10.41 mmol) were premixed in an internal mixer (Thermo Haake Rheocord Polylab 300p) for 10 min with a rotor speed of 60 rpm at 40 °C. Subsequently, the mixtures were pressed (Fontijne Holland Table Press TP 1000) with a force of 150 kN for 2 h at 140 °C. From the obtained sheets (2 mm), dumbbell test bars with the dimensions of 2 × 12.5 × 75 mm (DIN 53504-S2) or 1 × 6 × 35 mm (DIN 53504-S3) were punched out. The preparation of **2a**, **2c**, and **2d** was performed accordingly. In order to reduce the extent of early polymerization of **1e**, the pressing temperature for the preparation of **2e** was reduced to 100 °C. The as-prepared samples were subjected to mechanical testing and to solid-state ^{1}H NMR measurements. For recording high-resolution solution ^{1}H NMR spectra, unreacted alkylimidazoles were removed by reprecipitation. In order to ensure comparability, we have also checked the effect of high-temperature treatment of pure BIIR at 140 °C. Using the low-resolution NMR method described below, no change in the chain dynamics indicative of either degradation or thermal cross-linking was detected. Only heating significantly above 140 °C for extended amounts of time lead to degradation effects (possibly chain scission) in all samples.

*In Solution (**2e$_s$**).* An amount of 30 g of BIIR (4.24 mmol of allylic bromide) was dissolved in 300 mL of methylene chloride at room temperature. Subsequently, **1e** (0.98 g, 4.24 mmol) was added in equimolar ratio. After a reaction time of 3 days at room temperature, the mixture was heated up to 65 °C and stirred for a further 3 days. After evaporation of the solvent, the product was dissolved in toluene and precipitated in acetone. The resulting precipitate was filtered off, washed several times with acetone, and dried several days at 100 °C under reduced pressure. A sample overview is given in Table 1.

Sulfur Cross-Linking of BIIR. For comparison purposes, BIIR was sulfur cross-linked following a conventional compounding recipe. Details were described in a previous publication.[28] The sample obtained (BIIR-s) resembles very much a commercial rubber and served as reference to the alkylimidazole-modified BIIR samples **2a−2e**.

Instruments. Tensile tests were carried out on a Zwick 1456 tensile tester with a rate of elongation of 200 mm/min according to DIN EN ISO 527-2/S2/20.

Dynamic mechanical analysis (DMA) was performed on standard test bars with a dimension of 35 × 10 × 2 mm with a dynamic mechanical thermal spectrometer (Eplexor 200N, GABO QUALIMETER). The temperature-sweep measurements were performed at a frequency of 10 Hz and a heating rate of 2 K/min from −80 to 140 °C.

High-resolution solution ^{1}H NMR (500.13 MHz) spectra were recorded on an Avance III 500 NMR spectrometer (Bruker). $CDCl_3$ ($\delta(^1H)$ = 7.26 ppm) was used as solvent and internal standard.

Low-resolution, time-domain solid-state ^{1}H NMR measurements were performed on a Bruker Minispec mq20 benchtop spectrometer (B_0 = 0.47 T) with 90° and 180° pulses of 1.6 and 3.3 μs length, respectively. The used multiple-quantum (MQ) NMR experiment is based on the pulse sequence designed by Baum and Pines[33] as applied for a specific double-quantum (DQ) evolution time τ_{DQ}. Each intensity data point was obtained as an average over the initial, hardly decaying part of the free induction decay (FID) detected on-resonance after the applied MQ pulse sequence and a 90° read-out pulse.

Self-Healing Tests. For self-healing experiments, standard test specimens (DIN 53504 S2) were punched out of molded sheets. The experiments were performed with a custom-built test device[34] which ensured reproducibility (see Figure 1). This device consists of two brass blocks with countersinks (a) which can be loaded simultaneously with three dumbbell test bars (b). Between the brass blocks is a 2 mm wide gap (c) in which the samples can be cut reproducibly. One brass block can be moved with a micrometer screw (d) in both directions. A cover (e) makes sure that the samples are fixed during the tests.

In a typical healing experiment, the test bars are introduced into the countersinks and cut with a razor blade within the gap area. Immediately thereafter, the cut sections are separated from each other and then pressed together with a defined compression of 0.1 mm. In this state, the samples are allowed to heal for 16 h at 70 °C and then stored at room temperature. Finally, the mended samples are subjected to tensile tests. For this, the engineering stress $\sigma = P/A_0$ was measured as a function of the strain $\varepsilon = l/l_0$, where P is the

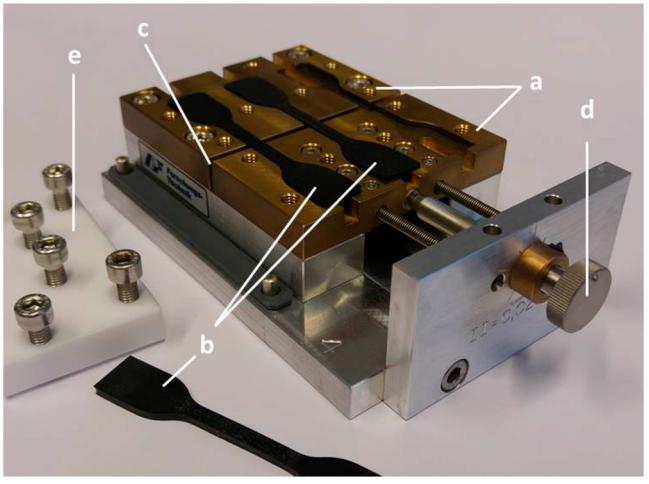

Figure 1. Custom-built test device for self-healing tests: (a) two brass blocks with three countersinks, (b) dumbbell test bars, (c) 2 mm wide cutting zone, (d) micrometer screw, and (e) Teflon cover.

DOI: 10.1021/acs.macromol.7b02287
Macromolecules 2018, 51, 468−479

applied load, A_0 is the original cross-sectional area, l is the measured length, and l_0 is the original length. The tensile stress (σ_b) and elongation at break (ε_b)-related healing efficiencies H_σ and H_ε were calculated as follows: $H_\sigma = \sigma_{b(h)}/\sigma_{b(v)} \times 100\%$ and $H_\varepsilon = \varepsilon_{b(h)}/\varepsilon_{b(v)} \times 100\%$ where $\sigma_{b(h)}$ and $\varepsilon_{b(h)}$ are the tensile stress and elongation at break values of the healed samples, respectively, and $\sigma_{b(v)}$ and $\varepsilon_{b(v)}$ are the tensile stress and elongation at break values of the virgin samples, respectively. Tensile properties and healing efficiencies are summarized in Table 2.

Table 2. Tensile Properties and Healing Efficiencies of Ionically Modified BIIR

sample	M[a]	$\sigma_{b(v)}$[b] [MPa]	$\varepsilon_{b(v)}$[c] [%]	H_σ[d] [%]	H_ε[e] [%]
2a	**1a**	16.9 ± 2.9	980 ± 30	18 ± 13	50 ± 30
2b	**1b**	12.3 ± 2.3	990 ± 70	25 ± 16	69 ± 20
2c	**1c**	10.7 ± 1.6	1040 ± 20	74 ± 43	98 ± 7
2d	**1d**	11.8 ± 2.6	1050 ± 20	57 ± 39	91 ± 11
$\mathbf{2e_i}$	**1e**	2.4 ± 0.7	1060 ± 60		
after 2 months		2.3 ± 0.7	940 ± 100		
$\mathbf{2e_{ii}}$	**1e**	4.5 ± 0.4	1110 ± 30	15 ± 3.7	24 ± 5
after 2 months		7.7 ± 1.5	990 ± 30		
$\mathbf{2e_{iii}}$	**1e**/**1b**	7.2 ± 0.6	1010 ± 10		
after 2 months		11.6 ± 1.8	940 ± 20		
BIIR-s[f]		7.0 ± 1.6	930 ± 30		

[a]Alkylimidazole used for modification. [b]Average tensile stress at break of the virgin samples. [c]Average elongation at break of the virgin samples. [d]Healing efficiency related to the tensile stress at break. [e]Healing efficiency related to the elongation at break. [f]BIIR was cross-linked by sulfur vulcanization.[28]

RESULTS AND DISCUSSION

Synthesis and Chemical Structure. The modification of BIIR with various alkylimidazoles (**1a**−**1e**) according to Scheme 1 was performed in the melt. In a typical example, BIIR and a 1.5-fold excess of imidazole (with reference to the number of bromide groups) were premixed at 40 °C. At this temperature the extent of grafting was low. Then, the samples were pressed for 60 min at 100 °C ($\mathbf{2e_{i-iii}}$) or for 2 h at 140 °C (**2a**−**d**). During pressing the grafting took place. In order to prevent side reactions and to achieve maximum conversion, grafting was also performed in solution ($\mathbf{2e_s}$). The olefinic region of the ^{1}H NMR spectra of BIIR, **2a**, **2c**, and $\mathbf{2e_s}$ is shown in Figure 2. Unconverted imidazoles and additives in BIIR, **2a**, and **2c** were removed by reprecipitation prior to the measurements. The signal assignment was made according to Parent et al.[22,35,36] The spectra of all samples exhibit a characteristic triplet at 5.1 ppm (H^1) which can be assigned to non-brominated isoprene units.[36] Since this group does not take part in the reaction, it can be used as internal standard. The spectrum of **2c** (see Figure 2c) resembles very much those of **2b** and **2d** (see Supporting Information: S5 and S6). For **2a**, the signals H^9, H^{11}, and H^{13} are slightly upfield shifted because of the influence of the CH_3 group.

The spectrum of BIIR (see Figure 2a) is dominated by the three signals of the exomethylene units (H^{2-4}) which diminished almost completely after conversion with the alkylimidazoles. According to Parent et al.,[22] the exomethylene units isomerize during the conversion into the more reactive endo-bromomethyl groups, the signals of which (H^5, H^7) can be found in the spectra of **2a**−**2d** in traces. The low signal intensities of H^{2-5} and H^7 exhibit that the modification of BIIR with the alkylimidazoles **1a**−**1d** proceeds almost quantitatively in the melt. From the signal intensities, the grafting degree (GD) was approximated to be higher than 95% (see Table 1).

The ^{1}H NMR spectroscopic characterization of **2e** was less straightforward. Owing to the possibility that alkylimidazole **1e** is able to polymerize, different imidazole and imidazolium structural units may be formed during the conversion. Especially, grafted and ungrafted chains of an oligomeric poly(ionic liquid) can be expected. In order to facilitate spectral interpretations, the conversion of BIIR with **1e** was performed first in $CHCl_3$ solution to yield the sample $\mathbf{2e_s}$. Ungrafted components were removed by reprecipitation of the sample in toluene/acetone. The spectrum of $\mathbf{2e_s}$ is shown in Figure 2d. The typical signals of the grafted sites H^{9-11} and H^{13-14} appeared at the same positions as for **2b**−**2d**. Furthermore, distinct signals of unconverted endo-bromomethyl groups (H^{5Br}, H^7) were found. Surprisingly, an additional signal (H^{5Cl}) appeared which was assigned to an endo-chloromethyl group. The assignment was based on a spectrum of isomerized CIIR.[35] The two signals at about 3.55 and 3.43 ppm could be assigned to halide terminal groups CH_2−X (H^{12}) of the grafted sites. Also here, beside the signal of the expected chlorine terminal group, an additional signal of a bromide terminal group appeared. Obviously, halide exchange reactions occurred during the conversion which resulted into a mixed halide substitution at the polymer chain and at the chain end of the grafted sites. This halide exchange probably takes place according to the Finkelstein mechanism, in the course of which the halides of the primary alkyl halide groups and the imidazolium salts are exchanged (see Scheme 2).

Based on the signal intensities I(H^{9+13}), I(H^{5Br+7}), I(H^{5Cl}), and I(H^{11}), the grafting degrees (GD) and the average grafting lengths (L) were calculated (see Table 1). For the calculation of L, only the grafted sites were taken into account. As further characteristics of **2e**, the ratio of bromine and chlorine substituted isoprene units (Br_{Is}/Cl_{Is}) and the ratio of the bromide and the chloride terminal groups of the grafted sides (Br_t/Cl_t) were calculated from the intensity ratios I(H^{5Br+7}):I(H^{5Cl}) and I(H^{12Br}):I(H^{12Cl}), respectively (see Table 1). Both ratios provide indications for the extent of halide exchange reactions during the modification.

The equimolar conversion of BIIR with **1e** in solution ($\mathbf{2e_s}$) yielded a relatively high grafting degree of 59%. In an analogous reaction in the melt ($\mathbf{2e_i}$), the grafting degree was only 19%. Obviously, the bromide groups in BIIR were better accessible in solution. With grafting lengths slightly above unity, the polymerization at the grafting sites was only of secondary importance. For modifications in the melt ($\mathbf{2e_{i-iii}}$), GD and L increased distinctly at higher amounts of alkylimidazoles. Best results were obtained for $\mathbf{2e_{iii}}$, which was obtained after simultaneous conversion with 1.5 equiv of **1e** and 1.0 equiv of **1b**. The actual motivation to use both monomers was to increase the grafting density along the polymer chain and to limit the number of still reactive groups in the final product.

Unreacted alkylimidazoles and noncovalent bonded oligomers are not included in the balance so far. Nevertheless, such species were present in the as-prepared samples but were removed by reprecipitation for a better assessment by ^{1}H NMR. A true quantification of these portions by NMR is difficult because of signal overlap. A qualitative indicator is provided by the signal at about 3.9 ppm, which can be assigned to the vicinal CH_2 group of an unreacted alkylimidazole

DOI: 10.1021/acs.macromol.7b02287
Macromolecules 2018, 51, 468−479

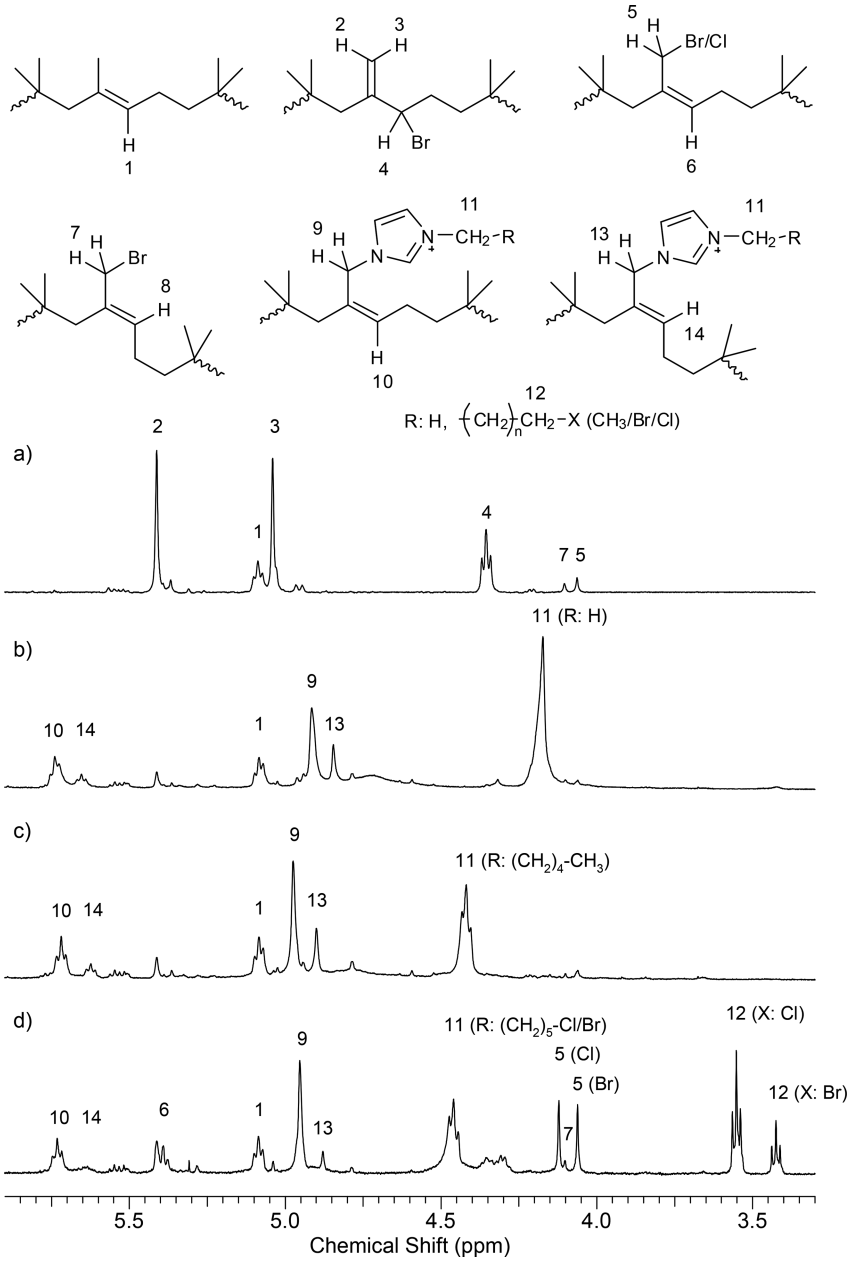

Figure 2. ^{1}H NMR spectra of (a) bromobutyl rubber, (b) **2a**, (c) **2c**, and (d) **2e$_s$** in $CDCl_3$. Signal assignment according to Parent et al.[22,35]

moiety. An example is given in the Supporting Information (S7). This signal decreased significantly after about 2 months storage of the samples at room temperature (Supporting Information S8). Simultaneously, the GD and *L* values increased (see Table 1), showing that the reactions were not complete after processing but continued during storage. Within this time unbound imidazole portions are successively incorporated in the growing side chain or directly bond to the BIIR backbone. All reactive species present in the system with altering portions are shown in Scheme 3. The influence of this slowly progressing reactions on mechanical properties will be discussed later.

As already mentioned above, halide exchange reactions occurred between the bromide groups of the BIIR backbone and the chloride chain ends of the grafted sites mediated by the imidazolium groups (see Scheme 2). The Br_I/Cl_I and Br_T/Cl_T ratios listed in Table 1 exhibit that at high GD and *L* values (**2e$_{ii}$**, **2e$_{iii}$**) mainly the less reactive chloride groups remain in the rubber whereas bromine is expected to act as counterion in the imidazolium salt. This seems to be close to an equilibrium state. In contrast to this, the sample **2e$_s$**, which was synthesized in solution, has not reached the equilibrium yet. Here, bromine is preferably situated at the BIIR backbone whereas chlorine is preferably found as terminal group of the grafts. Obviously, solvation of the halide counterions slows down the halide exchange process.

Mechanical Behavior and Self-Healing. The mechanical performance and the self-healing behavior of the ionically modified BIIR samples were assessed on the basis of stress–strain measurements. Figure 3 shows the stress–strain behavior of virgin (black) and healed (read) test bars of the samples **2a**–**2d**. For the healing tests the samples were cut into two pieces and then allowed to heal for 16 h at 70 °C (for details see the Experimental Section). For each sample 3–5

DOI: 10.1021/acs.macromol.7b02287
Macromolecules 2018, 51, 468–479

Scheme 2. Halide Exchange Reactions during Grafting of Bromobutyl Rubber with 1e

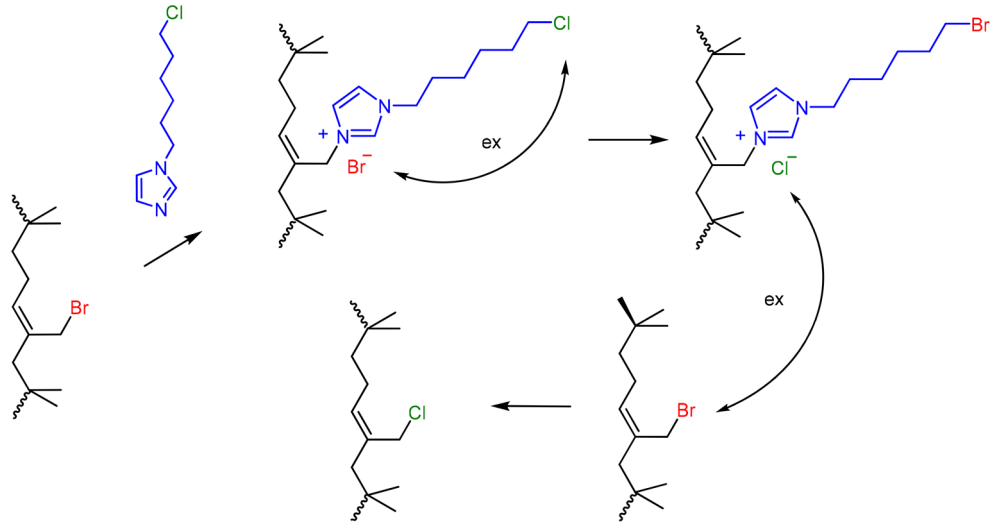

Scheme 3. Reactive Species in Bromobutyl Rubber Ionically Modified with 1e

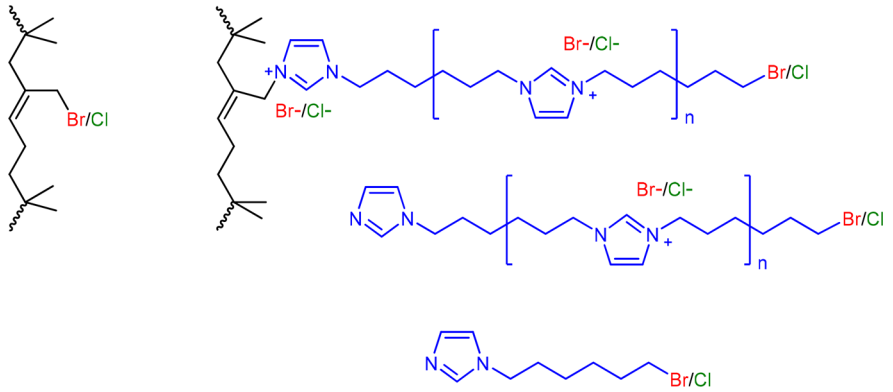

measurements were performed. The average values of the stress and elongation at break ($\sigma_{b(v)}$, $\varepsilon_{b(v)}$) as well as the healing efficiencies (H_σ, H_ε) are summarized in Table 2. For comparison purposes, the values of sulfur cross-linked BIIR are also listed.

Sample **2a** exhibited the highest average values of the stress at break with $\sigma_{b(v)}$ = 16.9 MPa, which is the sample with the shortest alkyl substituent at the imidazole graft. This is an excellent result for BIIR, taking into account that no covalent cross-linking occurred. The outstanding mechanical behavior is solely the result of an ionic network formation. With increasing length of the alkyl substituent, the stress at break values tended to decrease.

In contrast, the healing behavior of the samples exhibited a reverse tendency. With an average healing efficiency (H_σ = 18%, H_ε = 50%) the healing behavior of **2a** was only weakly pronounced, whereas the samples with longer alkyl substituents **2c** and **2d** exhibited very distinct healing levels (H_σ = 74% and 57%, H_ε = 98% and 91%, respectively). Obviously, the length of the alkyl substituents played an important role for the overall performance of ionically modified BIIR. Ionic groups with shorter substituents as in **2a** are assumed to form more compact clusters resulting in high mechanical strength. However, stronger interactions within the clusters also inhibit rearrangements of the ionic groups, resulting in a reduced healing efficiency in the case of damage. Longer alkyl substituents reduce the ionic interactions within the clusters. This exerts a positive effect on the healing behavior but at the same time decreases the mechanical performance. A very good compromise seems to be **2c** which shows pronounced self-healing at reasonable mechanical strength.

Selected stress−strain curves of BIIR modified with **1e** (samples $\mathbf{2e_i}$, $\mathbf{2e_{ii}}$, and $\mathbf{2e_{iii}}$) are shown in Figure 4. For comparison purposes the stress−strain curves of unmodified BIIR (a) and that of the covalently cross-linked BIIR-s (e) are also shown (for the whole set of stress−strain curves, see also Supporting Information: S9) . Owing to its lack of cross-links, the unmodified BIIR did not build up any significant tension during the experiment. In the ionically modified BIIR samples (b−d), the stress at break values increased with increasing amount of ionic groups; however, it did not exceed that of BIIR-s.

As already mentioned above, the reactions were not fully terminated after the conversion of BIIR with **1e**. Therefore, the samples were stored at room temperature for 2 months. During that time further reactions proceeded slowly. The influence of this progressing conversion on mechanical properties is demonstrated for $\mathbf{2e_{iii}}$ (see Figure 5). A distinct improvement of $\sigma_{b(v)}$ could be evidenced whereas $\varepsilon_{b(v)}$ slightly decreased. This effect could also be observed for $\mathbf{2e_{ii}}$, but on a distinctly lower initial level. The stress−strain curves of $\mathbf{2e_{iii}}$ after 2 months storage resembles those of **2c** and **2d**. Significant time-

DOI: 10.1021/acs.macromol.7b02287
Macromolecules 2018, 51, 468−479

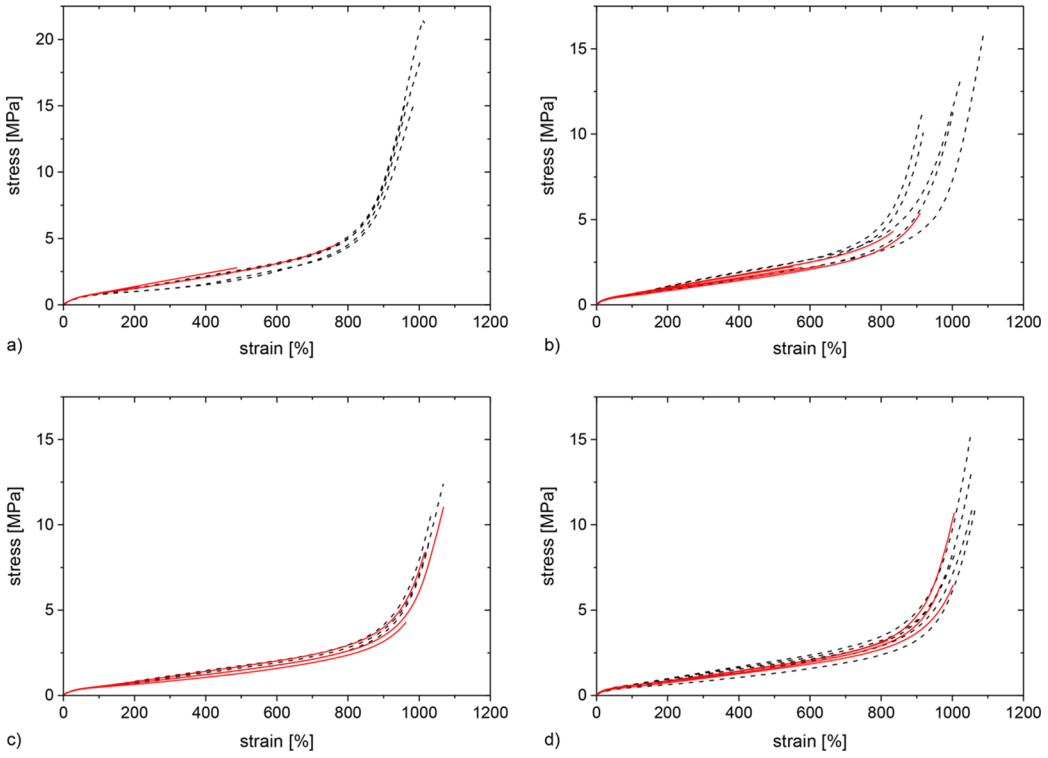

Figure 3. Stress−strain curves of (a) **2a**, (b) **2b**, (c) **2c**, and (d) **2d**. The black (dotted) and the red (solid) curves represent the virgin and the healed samples, respectively.

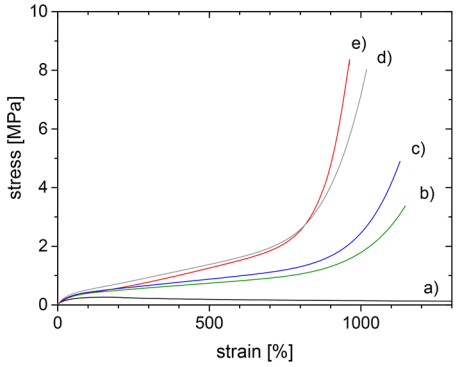

Figure 4. Selected stress−strain curves of (a) BIIR, (b) $\mathbf{2e_i}$, (c) $\mathbf{2e_{ii}}$, (d) $\mathbf{2e_{iii}}$, and (e) BIIR-s.

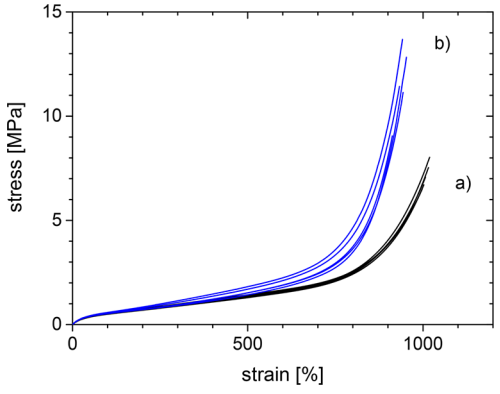

Figure 5. Stress−strain curves of $\mathbf{2e_{iii}}$: (a) virgin sample and (b) after 2 month storage at room temperature.

dependent changes in the stress−strain behavior of samples **2a−2d** have not been observed. This is demonstrated for **2b** in the Supporting Information (S10) as an example.

Surprisingly, the **2e** type samples exhibited no or only weakly pronounced self-healing, although the number of ionic groups was comparable with those of **2a−2d**. Obviously, the structural arrangement of the ionic groups plays an important role in terms of self-healing. Because of the ability of **1e** to polymerize, longer ionic grafts were formed during the modification of BIIR. For $\mathbf{2e_{ii}}$ and $\mathbf{2e_{iii}}$, the average grafting length L was approximately 2 (see Table 1). This is not very long but has obviously a critical influence on the size and strength of the ionic clusters. For a hypothetical cluster consisting of four ionic groups, the differences become clear from Scheme 4. From an energetic point of view, the release of

Scheme 4. Hypothetical Ionic Cluster Formation in Single Grafted BIIR (A) and Multiple Grafted BIIR (B)

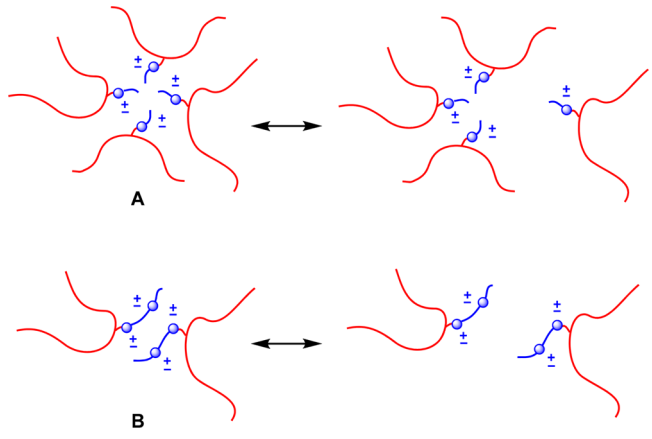

DOI: 10.1021/acs.macromol.7b02287
Macromolecules 2018, 51, 468−479

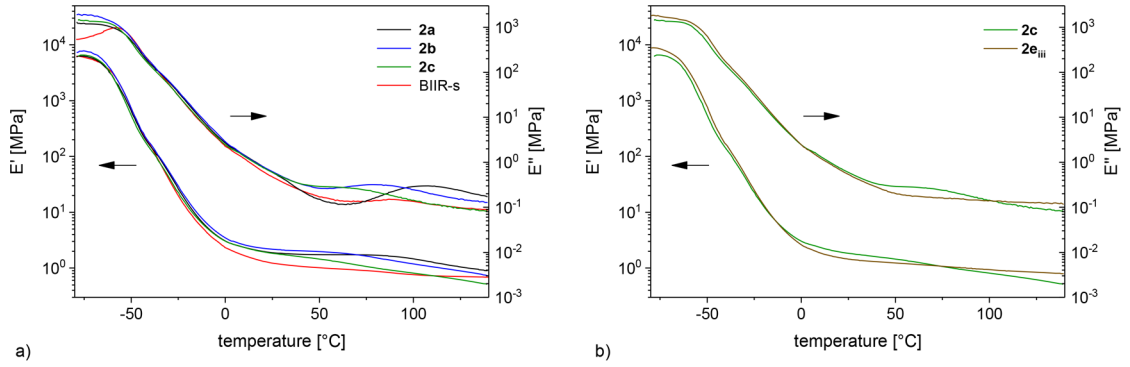

Figure 6. DMA temperature sweep test of (a) **2a**, **2b**, **2c**, and BIIR-s and (b) **2c** and **2e$_{iii}$**. The curves of **2d** (not shown) are congruent with those of **2c**.

one ionic group from cluster **A** should be easier than the separation of the ionic dimers from each other in cluster **B**. This suggests faster dynamics in the single grafted BIIR samples **2a**−**2d**. The stronger clusters in **2e** and the related reduced mobility of ionic groups are in our opinion the reason for the lack of self-healing.

The structural influence on the mechanical and self-healing behavior of modified BIIR could be confirmed by DMA measurements (see Figure 6). It should first be noted that the storage modulus E' of all single grafted samples **2a**−**2d** exceed above the glass transition that of the covalently cross-linked sample BIIR-s (see Figure 6a). This correlates well with the mechanical strength of the samples (see $\sigma_{b(v)}$ values in Table 2). Only at temperatures >100 °C, a reduction of the storage moduli below the level of BIIR-s is observed. This can be explained by a decrease of the cluster strength. This effect becomes more distinct with increasing length of the aliphatic substituent R at the imidazolium moieties. In the loss-modulus curves of **2a**−**2d**, a distinct relaxation is observed in the plateau region. This indicates fast chain dynamics in the ionic network. The maximum of this relaxation shifts to lower temperatures with increasing length of the aliphatic substituent. This is consistent with the assumption that longer aliphatic substituents reduce the cluster stability and hence, result in increased self-healing efficiency. Owing to the covalent linkages, the chain dynamics in BIIR-s are reduced at higher temperatures. Because of this reason, no self-healing is observed.

The dynamic mechanical behavior of **2e$_{iii}$** is shown in Figure 6b. Compared to **2c**, the drop in the storage modulus curve of **2e$_{iii}$** with increasing temperatures is distinctly less pronounced. The missing relaxation in the loss-modulus curve indicates a more restricted chain mobility. Taking into account the missing self-healing behavior and the dynamic mechanical behavior, **2e$_{iii}$** rather resembles BIIR-s than the other ionically modified samples. The reason for this is the strength of the ionic clusters which is assumed to be higher in **2e$_{iii}$** as already discussed above. The formation of strong clusters affects under this priority the material properties in a similar way as covalent cross-linking.

An additional influence might be caused by the nature of the counterions. It has been mentioned above that in **2e$_{iii}$** chloride appears as counterion besides bromide (see Scheme 3). The chloride anion is distinctly smaller than the bromide anion so that ionic clusters with chloride counterions are supposed to be more compact, resulting in higher cluster stability.

Molecular Dynamics−^{1}H MQ NMR. In order to rationalize the mechanical and self-healing behavior of ionically modified BIIR on a molecular basis, ^{1}H multiple-quantum (MQ) NMR experiments were performed. ^{1}H MQ NMR has been widely used to elucidate structural properties of various physical (entangled polymer melts), permanent, and ionic networks.[37−39] In these references, details on the pulse sequence and the processing of the measured signal functions are given. The relevant set of data obtained after some processing steps, which is the subject of further analyses, is the normalized double-quantum (DQ) buildup curve (I_{nDQ}); see Figure S11 in the Supporting Information for an example.

The buildup of DQ coherences relies on the existence of dipole−dipole couplings (DDCs) between the protons of all monomeric units, which are the target quantity characterizing the network structure (it should be noted that the isotropically mobile defect fraction, obtained in the course of the data analysis, was below 10% in all cases). DDCs are orientation-dependent and are averaged to zero in low-molecular-weight liquids and solutions. However, as a result of the weakly anisotropic rotations of a chain segment suspended between cross-links (chemical or physical), the DDCs average out to a certain low but finite level called residual DDC (RDDC), characterized by a coupling constant D_{res} (given in rad/s) reflecting the magnitude of motional anisotropy. This provides structural information in terms of the inverse effective length of the chain (the longer the chain, the lower D_{res}). Such motional anisotropy can be caused by different topological constraints such as entanglements, permanent, or supramolecular cross-links. In the case of permanent networks the DDCs average out to a constant D_{res} value set by the cross-link density. Clearly, the larger the cross-link density is the shorter is the part of the chain flanked by two cross-links, which makes it less mobile, resulting in a larger D_{res} value. In fact, D_{res} is directly proportional to the cross-link density. In the case of entangled polymer melts and supramolecular networks, the apparent cross-link density, and hence D_{res}, decreases with temperature because the polymer chain explores more space within the NMR time scale by overcoming the topological constraints (entanglements or supramolecular cross-links with a finite lifetime). Provided the samples are structurally homogeneous, that is, possess a narrow distribution of D_{res}, their I_{nDQ} signal can be analyzed by the following fitting function:[40]

$$I_{nDQ}(\tau_{DQ}, D_{res}) = 0.5(1 - \exp[-(0.378 D_{res}\tau_{DQ})^{1.5}] \times \cos[0.583 D_{res}\tau_{DQ}]) \quad (1)$$

DOI: 10.1021/acs.macromol.7b02287
Macromolecules 2018, 51, 468−479

However, in real-life samples one can expect a distribution. D_{res} distributions can be well addressed by the assumption of a log-normal distribution[41,42]

$$P(\ln(D_{res})) = \frac{1}{\sigma_{\ln}\sqrt{2\pi}} \exp\left[-\frac{(\ln(D_{res}) - \ln(D_{med}))^2}{2\sigma_{\ln}^2}\right] \quad (2)$$

where D_{med} is the median of the D_{res} distribution and $\sigma_{\ln}$ is the standard deviation on the $\ln(D_{res})$ scale.

The resulting fitting function reads[42]

$$I_{nDQ}(\tau_{DQ}) = \int (\ln(D_{res}))I_{nDQ}(\tau_{DQ}, D_{res})\, d\ln(D_{res}) \quad (3)$$

See Figure S11 for a sample fit. The extracted D_{med} values for all the samples are summarized in Figure 7.

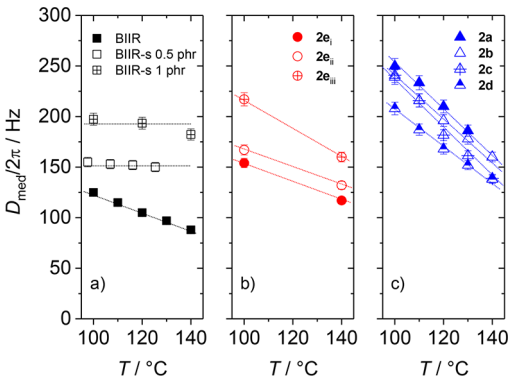

Figure 7. Structural information in the form of D_{med} extracted with eq 3 for (a) pristine BIIR and sulfur cross-linked BIIR-s as nonionic reference, (b) ionic networks **2e$_{i-iii}$** grafted with polymerizable 1-(6-chlorohexyl)-1*H*-imidazole **1e**, and (c) ionic networks **2a−2d** grafted with alkylimidazoles **1a−1d**.

In Figure 7a, one can see that the permanent BIIR-s networks, cross-linked conventionally with 0.5 and 1 phr sulfur, show temperature-independent plateaus because of time-stable chemical cross-links. As expected, a larger amount of used sulfur causes higher cross-link density and therefore larger D_{med}. In contrast to the cross-linked samples, the un-cross-linked BIIR sample exhibits long-range dynamics, as polymer chains can reptate, which leads to the decrease in D_{med}. The pure BIIR is multiply entangled (around 70 entanglements per chain according to its molar mass), and the fact that its normalized DQ buildup curves also reached the plateau value of 0.5 for long excitation time values indicates that the actual reptation regime (long-range dynamics), leading to significant time modulation of the instantaneous residual dipolar coupling on the DQ experimental time scale (with a power-law exponent of −0.5 for the dipolar correlation function), and thus signal loss, is not reached. In other words, the NMR experiments probe regime II of the tube model (local reptation or constrained Rouse motion).

Figure 7b depicts the D_{med} values of the ionic networks **2e$_{i-iii}$** grafted with the polymerizable modifier **1e**. The apparent cross-link density at 100 °C is initially higher than for the purely entangled BIIR and decreases with temperature through thermal activation of the ionic links. The level of the cross-link density (as defined by the number of ionic groups per chain) obviously exceeds the entanglement level, which is in line with the solution-state NMR results. Thus, the lifetimes of the ionic cross-links are initially longer than the relaxation time of the chain between two entanglements equilibrating through Rouse segmental motions, and both quantities are longer than the experimental NMR time scale at 100 °C.

In Figure 7c, the ionic networks **2a−2d** made by modification with alkylimidazoles varying in length of the alkyl group are compared. These samples also show pronounced thermal activation of the ionic links, as concluded

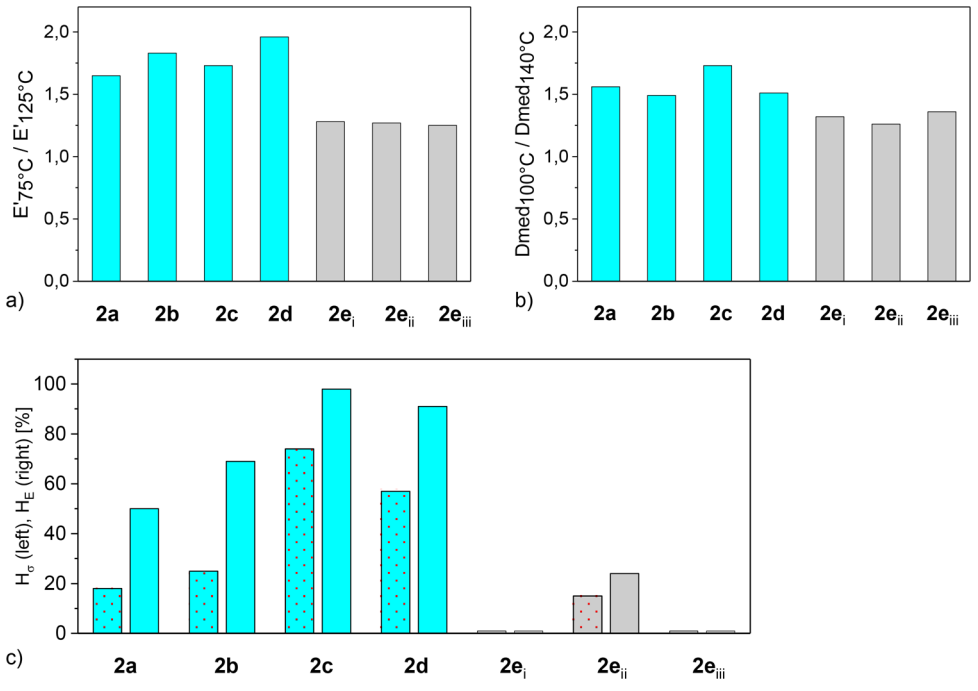

Figure 8. Comparison of rheological behavior, network chain dynamics assessed by NMR, and self-healing behavior of samples **2a−2e**: (a) ratios of the storage moduli at 75−125 °C; (b) ratio of the D_{med} values at 100−140 °C; (c) self-healing efficiencies H_σ and H_E.

DOI: 10.1021/acs.macromol.7b02287
Macromolecules 2018, 51, 468−479

from the strong decrease of D_{med} with temperature, but in a value range that again exceeds that of the non-cross-linked BIIR.

It can be seen that with length of the alkyl group the effective cross-link density and stability of the transient network decrease. This can be explained by impairing of ionic interactions by steric hindrance of the alkyl groups. Certainly, the larger the alkyl group is, the larger is the extent of screening of interacting ions. Thus, weaker interacting groups are more prone to open. As a result, polymer chains have more spatial freedom within the time scale of the NMR experiment (given by the shortest measured τ_{DQ} of about 50 μs), which leads to the additional averaging of DDCs and lower D_{med}. Compared to the ionic networks from Figure 7b, the initial apparent cross-link densities observed at 100 °C are larger. This is again defined by the degree of ionic modification, which is in the case of the alkylimidazole-modified samples much larger than for the samples modified with **1e**. However, the analysis of the thermal evolution of the ionic network structures implies that ionic links of the **2e** samples are more stable than ionic links of the alkylimidazole-modified samples **2a**−**2d**. This can be concluded from the lower D_{med} vs T slopes of the former samples as a qualitative indicator. This observation, obtained on the molecular scale, thus fortifies the aforementioned hypothesis that the longer grafting lengths (L) in $\mathbf{2e}_{i-iii}$ establish more strongly interacting ionic cross-links, since more ionic groups must be separated in this case, and also supports the findings from the self-healing tests. The smaller Cl^- anion, which shields the imidazole cation less than the larger Br^- anion, also contributes to stronger ionic interactions of $\mathbf{2e}_{i-iii}$.

On the whole, the dynamics reflected in these results is certainly complex, also involving distributions of ionic cluster sizes and bond lifetimes. A more in-depth analysis of the NMR results will thus be the subject of a forthcoming publication.

Correlations between Mechanical Properties, Molecular Dynamics, and Self-Healing Behavior. To illustrate the direct correlation between mechanical properties, molecular dynamics, and self-healing behavior more clearly, characteristic parameters of all samples obtained by DMA, ^{1}H MQ NMR studies, and the self-healing experiments are compared in Figure 8. The ratio of the moduli at 75 and 125 °C shown in Figure 8a and the ratio of the D_{res} values at 100 and 140 °C shown in Figure 8b represent measures for an increasing loss in mechanical strength and for increasing network dynamics in the respective temperature intervals. Note that the different absolute temperatures merely reflect the different frequency ranges probed by the different experiments (10 Hz for DMA vs inverse τ_{DQ} corresponding to the kHz range for NMR). In other words, in the given temperature range the modulus ratio reflects the observed distinct additional relaxation in the plateau region attributed to ionic groups, which in turn is probed by the NMR quantity as discussed above.

Comparing these values with the results of self-healing in Figure 8c, a clear correlation is evident. The group of samples $\mathbf{2e}_{i-iii}$ with a weaker tendency to self-healing is characterized by overall lower losses of mechanical strength as well as by time-stable network chains (comparably reduced relaxation dynamics) at higher temperatures. This confirms the above assumption about the influence of the strength of the ionic clusters and demonstrates the importance of mobility within the network to achieve self-healing behavior. The correlation of the individual behaviors within the sample group **2a**−**2d** is less clear and requires more detailed analyses of both the mechanical and the NMR data, since sample inhomogeneity (distributions of ionic cluster sizes and lifetimes) is likely relevant for these samples.

CONCLUSIONS

The ionic modification of BIIR yielded an elastomeric material, the overall properties of which were comparable with those of covalently cross-linked BIIR. The tensile properties even partially exceeded the level of sulfur cross-linked BIIR filled with silica or carbon black.[43] Additionally, a number of samples exhibited pronounced self-healing behavior. This unique spectrum of properties can be attributed to the formation of an ionic network. Obviously, the network is strong enough to give the material mechanical strength. At the same time, a sufficient dynamic of the network facilitates healing effects. We note that this specific kind of network dynamics can be attributed to the diffusion of a primitive chain through slip-links which represent the presence of entanglements and consider additionally the presence of weakly associating reversible cross-linkers on this kind of diffusion.[44] In qualitative accordance with our DMA results here, model calculations show that in contrast to a nonassociating entangled system the elastic modulus has a much higher first plateau and a delayed terminal relaxation. These effects are attributed to the evolution of the entangled chains as influenced by tethered reversible linkers.[44]

Both the tensile strengths and the healing efficiency are structurally influenced by the type of ionic groups and thus by the strength of ionic clusters formed. Here, the results point to an opposing influence. Whereas the formation of strong ionic clusters results in high mechanical strength, self-healing behavior rather demands faster chain dynamics which only occurs for weaker clusters. Particularly strong clusters are assumed in samples with short aliphatic substituents at the imidazolium moieties (**2a**) or with longer grafting sides (**2e**). These samples exhibited no or only weakly pronounced self-healing. The reduction of the cluster strength by introducing longer aliphatic substituents (**2b**−**2d**) resulted in pronounced self-healing without sacrificing mechanical performance much. Here, a compromise between mechanical performance and self-healing has been found. Sample **2c** with $\sigma_{b(v)}$ = 10.7 MPa, $\varepsilon_{b(v)}$ = 1040%, H_σ = 74%, and H_ε = 98% seems to be the optimum. Compared to other self-healing rubber like materials with noncovalent interactions,[1−13] the overall performance of the ionically modified BIIR described here is outstanding.

An important contribution to a better understanding of the relationships between macroscopic properties and molecular dynamics was provided by ^{1}H MQ NMR experiments. Based on temperature-dependent measurements of the level of residual dipole−dipole couplings characterizing length and time stability of network chains, the differences in mechanical behavior and their explanation in terms of peculiarities of the network formation via dynamic ionic clusters could be confirmed. A more quantitative analysis of the NMR data in terms of specific relaxation regimes ("sticky reptation") will be presented elsewhere.

Our results clearly show that self-healing rubbers are available by the utilization of ionic interactions and that these interactions can be finely tuned to the respective application. This regards structure, concentration, and distribution of the ionic groups, shielding effects caused by

DOI: 10.1021/acs.macromol.7b02287
Macromolecules 2018, 51, 468−479

flexible substituents as well as chain dynamics. Our initial intention to simply improve the self-healing behavior of BIIR by the formation of longer grafts of a poly(ionic liquid) was not successful, since the self-healing behavior disappeared for stronger clusters and consequently reduced chain dynamics. However, we expect that our strategy of tuning the interaction strength, possibly combined with the preparation of partially covalently linked hybrid networks, can aid in tailoring self-healing elastomers for real-life applications. In this context, it would be interesting to further assess the extent of reduction of the cluster strength by anion exchange in order to enhance the self-healing. This will be subject of further investigations.

■ ASSOCIATED CONTENT

Supporting Information

The Supporting Information is available free of charge on the ACS Publications website at DOI: 10.1021/acs.macromol.7b02287.

Determination of the allylic bromide content; high-resolution solution ^{1}H NMR spectra of **1c**, **1d**, **1e**, **2b**, **2d**, **2e**$_{iii}$ (as-prepared), and **2e**$_{iii}$ (after 2 month storage); additional stress−strain curves of **2b**, **2e**$_i$, **2e**$_{ii}$, **2e**$_{iii}$, and BIIR-s; solid state NMR: fitting of the I_{nDQ} signal of **2a** (T = 100 °C) (PDF)

■ AUTHOR INFORMATION

Corresponding Authors

*E-mail boehme@ipfdd.de (F.B.).
*E-mail kay.saalwaechter@physik.uni-halle.de (K.S.).

ORCID

Nikhil K. Singha: 0000-0003-0935-0157
Frank Böhme: 0000-0001-6128-4658

Notes

The authors declare no competing financial interest.

■ ACKNOWLEDGMENTS

This work was supported by the Deutsche Forschungsgemeinschaft (DFG, BO 1121/7-1, BO 1121/9-1, HE 4466/32-1, SA982/9-1) in the Priority Program (Schwerpunktprogramm), SPP 1568 "Design and Generic Principles of Self-Healing Materials". Thanks are due to DAAD for the fellowship for Ms. Manta Roy under the DAAD-IIT Sandwich program. The authors thank Dr. Hartmut Komber for the discussion of the solution NMR results, and Natalie König for performing some of the low-field NMR measurements.

■ REFERENCES

(1) Cordier, P.; Tournilhac, F.; Soulie-Ziakovic, C.; Leibler, L. Self-healing and thermoreversible rubber from supramolecular assembly. *Nature* **2008**, *451* (7181), 977−980.

(2) You, Y.; Huang, W. Y.; Zhang, A. Q.; Lin, Y. L. A Facile and Controllable Synthesis of Dual-Crosslinked Elastomers Based on Linear Bifunctional Polydimethylsiloxane Oligomers. *J. Polym. Sci., Part A: Polym. Chem.* **2016**, *54* (23), 3760−3768.

(3) Liu, L.; Pan, C.; Zhang, L. Q.; Guo, B. C. A Novel and Non-Cytotoxic Self-Healing Supramolecular Elastomer Synthesized with Small Molecular Biological Acids. *Macromol. Rapid Commun.* **2016**, *37* (19), 1603−1610.

(4) Grande, A. M.; Garcia, S. J.; van der Zwaag, S. On the interfacial healing of a supramolecular elastomer. *Polymer* **2015**, *56*, 435−442.

(5) Cheng, C. C.; Chang, F. C.; Chen, J. K.; Wang, T. Y.; Lee, D. J. High-efficiency self-healing materials based on supramolecular polymer networks. *RSC Adv.* **2015**, *5* (122), 101148−101154.

(6) Chen, S. B.; Mahmood, N.; Beiner, M.; Binder, W. H. Self-Healing Materials from V- and H-Shaped Supramolecular Architectures. *Angew. Chem., Int. Ed.* **2015**, *54* (35), 10188−10192.

(7) Xu, C. H.; Cao, L. M.; Lin, B. F.; Liang, X. Q.; Chen, Y. K. Design of Self-Healing Supramolecular Rubbers by Introducing Ionic Cross-Links into Natural Rubber via a Controlled Vulcanization. *ACS Appl. Mater. Interfaces* **2016**, *8* (27), 17728−17737.

(8) Hernandez, M.; Grande, A. M.; Dierkes, W.; Bijleveld, J.; van der Zwaag, S.; Garcia, S. J. Turning Vulcanized Natural Rubber into a Self-Healing Polymer: Effect of the Disulfide/Polysulfide Ratio. *ACS Sustainable Chem. Eng.* **2016**, *4* (10), 5776−5784.

(9) Kuang, X.; Liu, G. M.; Dong, X.; Wang, D. J. Enhancement of Mechanical and Self-Healing Performance in Multiwall Carbon Nanotube/Rubber Composites via Diels-Alder Bonding. *Macromol. Mater. Eng.* **2016**, *301* (5), 535−541.

(10) Wang, D.; Guo, J.; Zhang, H.; Cheng, B. C.; Shen, H.; Zhao, N.; Xu, J. Intelligent rubber with tailored properties for self-healing and shape memory. *J. Mater. Chem. A* **2015**, *3* (24), 12864−12872.

(11) Schüssele, A. C.; Nübling, F.; Thomann, Y.; Carstensen, O.; Bauer, G.; Speck, T.; Mülhaupt, R. Self-Healing Rubbers Based on NBR Blends with Hyperbranched Polyethylenimines. *Macromol. Mater. Eng.* **2012**, *297* (5), 411−419.

(12) Xiang, H. P.; Rong, M. Z.; Zhang, M. Q. Self-healing, Reshaping, and Recycling of Vulcanized Chloroprene Rubber: A Case Study of Multitask Cyclic Utilization of Cross-linked Polymer. *ACS Sustainable Chem. Eng.* **2016**, *4* (5), 2715−2724.

(13) Jia, X. Y.; Mei, J. F.; Lai, J. C.; Li, C. H.; You, X. Z. A Highly Stretchable Polymer that Can Be Thermally Healed at Mild Temperature. *Macromol. Rapid Commun.* **2016**, *37* (12), 952−956.

(14) Hernandez, M.; Grande, A. M.; van der Zwaag, S.; Garcia, S. J. Monitoring Network and Interfacial Healing Processes by Broadband Dielectric Spectroscopy: A Case Study on Natural Rubber. *ACS Appl. Mater. Interfaces* **2016**, *8* (16), 10647−10656.

(15) Das, A.; Le, H. H.; Vuorinen, J.; Heinrich, G. Comment on "Monitoring Network and Interfacial Healing Processes by Broadband Dielectric Spectroscopy: A Case Study on Natural rubber". *ACS Appl. Mater. Interfaces* **2017**, *9*, 14547.

(16) Parent, J. S.; White, G. D. F.; Whitney, R. A.; Hopkins, W. Amine substitution reactions of brominated poly(isobutylene-co-isoprene): New chemical modification and cure chemistry. *Macromolecules* **2002**, *35* (9), 3374−3379.

(17) Faba, M. A. J.; Parent, J. S.; Whitney, R. A. CO(2)-Derived Latent Nitrogen Nucleophiles for Controlled Cross-Linking of Brominated Poly(isobutylene-co-isoprene). *Polym. Eng. Sci.* **2011**, *51* (8), 1592−1598.

(18) Parent, J. S.; Malmberg, S.; McLean, J. K.; Whitney, R. A. Nucleophilic catalysis of halide displacement from brominated poly(isobutylene-co-isoprene). *Eur. Polym. J.* **2010**, *46* (4), 702−708.

(19) Xiao, S. D.; Parent, J. S.; Whitney, R. A.; Knight, L. K. Synthesis and Characterization of Poly(isobutylene-co-isoprene)-Derived Macro-Monomers. *J. Polym. Sci., Part A: Polym. Chem.* **2010**, *48* (21), 4691−4696.

(20) Faba, M. A. J.; Parent, J. S.; Whitney, R. A. Reactions of N-Alkylbenzaldimines with Brominated Poly(isobutylene-co-isoprene): New Delayed Onset Cure Chemistry. *Ind. Eng. Chem. Res.* **2011**, *50* (2), 680−685.

(21) Parent, J. S.; Malmberg, S. M.; Whitney, R. A. Auto-catalytic chemistry for the solvent-free synthesis of isobutylene-rich ionomers. *Green Chem.* **2011**, *13* (10), 2818−2824.

(22) Parent, J. S.; Porter, A. M. J.; Kleczek, M. R.; Whitney, R. A. Imidazolium bromide derivatives of poly(isobutylene-co-isoprene): A new class of elastomeric ionomers. *Polymer* **2011**, *52* (24), 5410−5418.

(23) Varley, R. J.; van der Zwaag, S. Development of a quasi-static test method to investigate the origin of self-healing in ionomers under ballistic conditions. *Polym. Test.* **2008**, *27* (1), 11−19.

(24) Rhaman, M. A.; Penco, M.; Spagnoli, G.; Grande, A. M.; Di Landro, L. Self-Healing Behavior of Blends Based on Ionomers with

DOI: 10.1021/acs.macromol.7b02287
Macromolecules 2018, 51, 468−479

Ethylene/Vinyl Alcohol Copolymer or Epoxidized Natural Rubber. *Macromol. Mater. Eng.* **2011**, *296* (12), 1119−1127.
(25) Kalista, S. J.; Ward, T. C. Thermal characteristics of the self-healing response in poly (ethylene-co-methacrylic acid) copolymers. *J. R. Soc., Interface* **2007**, *4* (13), 405−411.
(26) Kalista, S. J.; Pflug, J. R.; Varley, R. J. Effect of ionic content on ballistic self-healing in EMAA copolymers and ionomers. *Polym. Chem.* **2013**, *4* (18), 4910−4926.
(27) Kalista, S. J.; et al. Self-healing of poly(ethylene-co-methacrylic acid) copolymers following projectile puncture. *Mech. Adv. Mater. Struct.* **2007**, *14* (5), 391−397.
(28) Das, A.; Sallat, A.; Böhme, F.; Suckow, M.; Basu, D.; Wießner, S.; Stöckelhuber, K. W.; Voit, B.; Heinrich, G. Ionic Modification Turns Commercial Rubber into a Self-Healing Material. *ACS Appl. Mater. Interfaces* **2015**, *7* (37), 20623−20630.
(29) Le, H. H.; Hait, S.; Das, A.; Wiessner, S.; Stöckelhuber, K. W.; Böhme, F.; Reuter, U.; Naskar, K.; Heinrich, G.; Radusch, H. J. Self-healing properties of carbon nanotube filled natural rubber/bromobutyl rubber blends. *eXPRESS Polym. Lett.* **2017**, *11* (3), 230−242.
(30) Le, H. H.; Böhme, F.; Sallat, A.; Wießner, S.; Landwehr, M. A. D.; Reuter, U.; Stöckelhuber, K. W.; Heinrich, G.; Radusch, H. J.; Das, A. Triggering the Self-Healing Properties of Modified Bromobutyl Rubber by Intrinsically Electrical Heating. *Macromol. Mater. Eng.* **2017**, *302* (4), 1600385.
(31) Suckow, M.; Zschoche, S.; Heinrich, G.; Voit, B.; Böhme, F. New reactive poly(ionic liquid)s synthesized by polymer analogous conversion of maleic anhydride containing polymers. *Polymer* **2016**, *96*, 20−25.
(32) Suckow, M.; Roy, M.; Sahre, K.; Häußler, L.; Singha, N. K.; Voit, B.; Böhme, F. Synthesis of polymeric ionic liquids with unidirectional chain topology by AB step growth polymerization. *Polymer* **2017**, *111*, 123−129.
(33) Baum, J.; Pines, A. Nmr-Studies of Clustering in Solids. *J. Am. Chem. Soc.* **1986**, *108* (24), 7447−7454.
(34) Suckow, M.; Stein, S.; Körber, V.; Grohmann, E. Verfahren und Vorrichtung zur Herstellung von Probekörpern für die Untersuchung selbstheilender Eigenschaften von Polymeren. DE 10 2016 208 745.2, **2016**.
(35) McNeish, J. R.; Parent, J. S.; Whitney, R. A. Halogenated poly(isobutylene-co-isoprene): influence of halogen leaving-group and polymer microstructure on chemical reactivity. *Can. J. Chem.* **2013**, *91* (6), 420−427.
(36) Cheng, D. M.; Gardner, I. J.; Wang, H. C.; Frederick, C. B.; Dekmezian, A. H.; Hous, P. Spectroscopic Studies of the Structures of Butyl and Bromobutyl Rubbers. *Rubber Chem. Technol.* **1990**, *63* (2), 265−275.
(37) Chávez, F. V.; Saalwächter, K. Time-Domain NMR Observation of Entangled Polymer Dynamics: Universal Behavior of Flexible Homopolymers and Applicability of the Tube Model. *Macromolecules* **2011**, *44* (6), 1549−1559.
(38) Saalwächter, K. Proton multiple-quantum NMR for the study of chain dynamics and structural constraints in polymeric soft materials. *Prog. Nucl. Magn. Reson. Spectrosc.* **2007**, *51* (1), 1−35.
(39) Malmierca, M. A.; González-Jiménez, A.; Mora-Barrantes, I.; Posadas, P.; Rodríguez, A.; Ibarra, L.; Nogales, A.; Saalwächter, K.; Valentín, J. L. Characterization of Network Structure and Chain Dynamics of Elastomeric Ionomers by Means of H-1 Low-Field NMR. *Macromolecules* **2014**, *47* (16), 5655−5667.
(40) Chassé, W.; Valentín, J. L.; Genesky, G. D.; Cohen, C.; Saalwächter, K. Precise dipolar coupling constant distribution analysis in proton multiple-quantum NMR of elastomers. *J. Chem. Phys.* **2011**, *134* (4), 044907.
(41) Lorthioir, C.; Randriamahefa, S.; Deloche, B. Some aspects of the orientational order distribution of flexible chains in a diblock mesophase. *J. Chem. Phys.* **2013**, *139* (22), 224903.
(42) Jakisch, L.; Garaleh, M.; Schäfer, M.; Mordvinkin, A.; Saalwächter, K.; Böhme, F. *Macromol. Chem. Phys.*, DOI 10.1002/macp.201700327.
(43) Dutta, N. K.; Tripathy, D. K. Effects of Types of Fillers on the Molecular Relaxation Characteristics, Dynamic Mechanical, and Physical-Properties of Rubber Vulcanizates. *J. Appl. Polym. Sci.* **1992**, *44* (9), 1635−1648.
(44) Mateyisi, M. J.; Sommer, J. U.; Müller-Nedebock, K. K.; Heinrich, G. Influence of weak reversible cross-linkers on entangled polymer melt dynamics. arXiv:1712.03868 [cond-mat.soft].

DOI: 10.1021/acs.macromol.7b02287
Macromolecules 2018, 51, 468−479